Scientific Research Publishing

Advances in Materials Physics and Chemistry, 2022, 12, 221-239
https://www.scirp.org/journal/ampc
ISSN Online: 2162-5328
ISSN Print: 2162-531X

Adsorbents for Gas Storage: Gas Energy, Sorbent Energy and Their Relationship to Capacity

Leonid Titelman

Department of Chemical Engineering, Ben-Gurion University of the Negev, Beer Sheva, Israel
Email: Titelman_leonid@hotmail.com

How to cite this paper: Titelman, L. (2022) Adsorbents for Gas Storage: Gas Energy, Sorbent Energy and Their Relationship to Capacity. *Advances in Materials Physics and Chemistry*, **12**, 221-239.
https://doi.org/10.4236/ampc.2022.1210016

Received: September 5, 2022
Accepted: October 24, 2022
Published: October 27, 2022

Abstract

Generalized variables make it possible to reveal the nuances of the structure of porous materials and divide samples into their series with similar properties (Titelman, L. AMPC 2021, vol. 11, No. 11). Adsorbents for gas storage have a unique set of variables that can be combined: textural and mechanical properties of the adsorbent, preparation conditions, pressure and temperature of gas during storage and delivery. Taking gas pressure and mechanical strength as forces, textural properties as displacements, we obtained the energies of gas and sorbent as generalized variables. The interrelationships between them and the storage capacity for metal-organic frameworks, porous organic polymers and activated carbons were studied. Due to the variety of sorbents and the attracting effect of micropore walls on gas adsorption, the previously proposed average thickness of the probing gas layer is useful as estimation of the pore size. Its effect on adsorbent capacity was tested. The ratio of the gas layer to the kinetic diameter of the molecule gives the packing of molecules inside the pores and makes it possible to represent the pore model. Excessive surface area results in too small pores, repulsive forces and reduced capacitance. Sometimes the gas energy correlates better with the residual adsorption uptake than with the total or delivery capacity. Compared to texture parameters, the proposed generalized variables correlate better with sorbent capacity.

Keywords

Generalized Parameter, Gas Energy, Sorbent Energy, Number of Gas Layers, Porous Materials

1. Introduction

This article focuses on the generalized properties (GPs) of adsorbents for gas

storage (StA); GPs were expected to correlate well with sorbent deliverable capacity. It has recently been shown [1] that the GPs (variables, parameters) of porous materials (PMs) behave like similarity numbers in completely different areas of nature (hydraulics, heat and mass transfer, geometry, etc.). The advantage of generalized variables in many-factorial experiments and series is the simultaneous consideration of changes in all single variables included in the generalized one. The GP proposal [2] was based on the identified earlier fact of the selective influence of technological variables (temperature, pressure, reagents, time) on various indicators of the mechanical strength of molded catalysts [3]. Later, it was extended to the textural properties of various PMs [2]. Combining two or more parameters into one GP allows revealing the nuances of the PM texture and dividing the samples into their series with similar properties. PMs include adsorbents and catalysts, both disordered and ordered [1] [2].

An interesting object for the use of GPs is currently relevant physical adsorbents for gas storage. As a rule, both the processing parameters (pressure P and temperature T) and textural parameters of the sorbent are involved in StA studies. When any process variable changes, it produces work, which is the product of force (P) and displacement in size or shape [2]. The textural properties (displacements) of the sorbent include total surface area (S_{BET}), total pore volume (V_p), and pore size distribution (PSD).

StAs include a wide range of materials: disordered and ordered activated carbons (ACs), metal-organic frameworks (MOFs), porous organic polymers (POPs), etc. These materials have narrow (micro-, ultra-micro-) pores in common. In AC, opposite walls enhance the attraction of adsorbate molecules (the overlapping effect [4]). This effect avoids both the very high pressure and very low (cryogenic) temperature needed to store gases such as H_2 and CH_4. Sethia and Sayari [5] report this effect at a pore size 0.6 ÷ 0.7 nm for H_2-AC pair; for the CH_4-AC pair, we found that the effect of the carbon pore size is manifested itself in the region of less than 1.3 nm ([1], Fig. 8). In MOF, the interpenetration of two or more sublattices in the same framework divides large pores into small ones, which increases its efficiency in storing CO_2 [6]. Unfortunately, in works devoted to gas storage adsorbents, the pore diameter D_p is rarely given. The variety of sorbents makes it difficult to choose some universal pore size model. It seems that the recently proposed [1] $\tau = V_p/S_{BET}$, the average thickness of the probing gas layers, can be tested for the role of the *universal* pore size for any porous material.

Generally, total capacity (absorption) at storage pressure and temperature and gas delivery (excess) capacity G at supply pressure and temperature are given. Capacities are measured in g or cm^3 of stored gas per unit (per gram, gravimetric G, g/g, per cm^3 or L, volumetric G, cm^3/cm^3) of either sorbent (option 1) or installation (option 2). The 1-st option is important for the scientific basis for the preparation of sorbents and catalysts, the 2-nd option is used for economic evaluations [7]. In this work, *the* 1st *option* will be used.

The dimension of gravimetrical uptake (G, g/g) contains a gram of sorbent. Recently [1], using the micropore volume V_{mi} (cm^3/g) of PM as an example, we have shown that the fluctuations of V_{mi} in a series of samples depend both on the fluctuations of the surface itself and the density of the adsorbent. The latter was found to be a redundant variable and eliminated by dividing V_{mi} by S_{BET}, *i.e.*, measuring V_{mi} in cm^3/m^2, which gives a noticeable reduction in the standard deviation (STD, %) of V_{mi} in a series of experiments. In addition, the STD itself becomes a serial GP. The V_{mi}/S_{BET} ratio is also a GP, a characteristic of the surface topography and a kind of roughness [1]. Note that study of the dependences G, g/g, both on S_{BET}, m^2/g, and on V_p, cm^3/g, is correct since both independent and dependent variables refer to the same gram of material. The idea of using *other dimensions of G instead* g/g will also be used in the current paper.

Fiero *et al.* [8] separated the effects of attraction of gas molecules and gas pressure ([8], Fig. 6: G, g/g, vs. S_{BET}): the amount of hydrogen stored by AC increases significantly due to adsorption only at moderate pressure: 3 MPa/298K and 0.15 MPa/77K, but at *high pressure*, the proportion of adsorbed gas is much less than that of just compressed gas ([8], Figs. 7, 31). Moreover,an increase in S_{BET} after a certain value led to a decrease in gravimetric G; this phenomenon was observed both at low (3 MPa) and high (20 MPa) pressures ([8], Fig. 6). The same phenomenon was previously noted by Goldsmith *et al.* [9]. *The objectives of this work are*: 1) to find the cause of the phenomenon, 2) not to separate, but to combine the parameters of gas pressure and adsorbent texture into generalized variables and evaluate the strength of their correlation with gas adsorption.

A small pore size often indicates a small dimensionless pore shape factor $F_d = D_p^* S_{BET}/V_p$ [1]. F_d values in range < 2 were found [https://doi.org/10.3762/bxiv.2020.89.v] among MCM-41 samples when the work of Putz *et al.* [10] was discussed. These samples, according to the conclusion of the authors of [10], have a disordered structure. Recall that the factor $F = 2000$, nm^*m^2/cm^3, or the dimensionless $F_d = 2$ [1] refers to the split pore model in the expression for the average hydraulic pore diameter $D_h = F_d^* V_p/S_{BET}$. Adsorbents with small split pores and parallel flat walls obviously create good conditions for the physical adsorption of gases. However, Gun'ko *et al.* [11], Azevedo *et al.* [12] note that the model of a flat slotted pore does not always allow one to describe the experimental data. For ACs, a model of mixed geometry was proposed [12], which represents the pore space as a set of an indefinite ratio of slit-like and triangular pores. Cardenas *et al.* [13] proposed "infinitely long pores with a polygonal (triangle, square, pentagon, hexagon, octagon, decagon, and circle) cross sections", including pores less than 1 nm in diameter, but they did not include a split shape. It is also very hard to predict the shape of MOF pores due to their large-scale flexibility, the presence of defects, and long-range disorder [14]. We expect that by applying the thickness of *probing gas layers* $\tau = V_p/S_{BET}$ we will be able to better appreciate the shape of the pores. This is *the next goal* of this work.

2. Generalized Energy Parameters of Storage Adsorbents

2.1. Two Forms of Energy in Porous Materials

When studying gas StA, a certain volume of either a storage container or sorbent pores is given, as well as pressure and temperature of the gas. The product of the gas volume V and the pressure P in a closed vessel at a constant temperature T

$$\left(PV\right)_T = \text{const} \tag{1}$$

is the equation of state for an *ideal* gas.

In a broad sense, PV is energy (work), where P is force and V is displacement [2]. In the case of a real gas, PV is a natural *generalized variable* whose deviation from constancy indicates the presence of additional variables (proximity to critical points, molecular dissociation, etc.). In the case of gas storage, an additional variable may be the forces of gas attraction (physical sorption) in narrow pores (overlapping effect [4]). *This effect can be fixed by the inversely proportional dependence of the capacitance on the pore size.* For a porous material, any textural property (pore volume V_p, surface area S_{BET}, and pore size) can serve as the displacement V in Equation (1). The force in the gas phase is pressure P. To go to the energy of the solid part of the sorbent, imagine a closed container, for example, a children's rubber balloon, on the walls of which a strain gauge is glued. As the gas pressure increases, the elongation and wall stress will increase until the balloon bursts. Let us change in Equation (1) the pressure of the gas P that destroys the cylinder by a certain tensile strength of its material P_m (the subscript $_m$-mechanical). So, the equation of state will be

$$\left(P_m V\right) = \text{const} \tag{2}$$

and $P_m V$ can be called the energy of the sorbent. This is an example of a process (P_m) - structural (V) generalized variable. Previously [SI-1] for a granule of a porous material, the mechanical strength of the pore walls was accepted as a result (as replica) of gas (steam) pressure that occurs inside the pores of the material during its preparation or operation; the gas pressure leading to the destruction of the wall corresponds to the crushing strength of the wall P_m. In practice, such destruction of the walls of the pores occurs when the high pressure in the catalyst bed is abruptly released or when the wet granules are dried too intensively.

$P_m V$ was expected to be constant over a range of process variables in the production of molded materials. P_m was a type of mechanical strength, depending on the loading scheme (device). The choice of the appropriate pore volume (total V_p, meso-V_{me}, micro-V_{mi}, etc.) was based on the statistical nature of the crushing of the catalyst tablets under uniaxial compression, each tablet is crushed differently. One of the statistical theories of strength, the theory of the weak link-says that the destruction begins from the weakest point in the product and then develops catastrophically. This point can be in the wall of a pore of any size, so every kind of pore volume V must be tested. Indeed, for many materials

and loading schemes (tables in SI-1) existence of $P_m V \approx$ const in the dependences of $P_m V$ on x (x is a technological variable) has been established. In the current paper, we have added S_{BET} surface area and pore size, either represented by D_p or by generalized V_p/S_{BET}, as displacements.

2.2. Pore Shape Factor as Number of Gas Layers

Taking into account that V_p/S_{BET} is the average thickness τ (nm) *of the probing gas layer* (usually N_2) and having the average pore diameter D_p, one more meaning of the *dimensionless pore shape factor* F_d can be found. From the "equation in separated generalized variables" for the average pore diameter [1] we obtain the pore shape factor

$$F_d = D_p \Big/ \left(V_p / S_{BET}\right) \tag{3}$$

Thus, the shape factor F_d has *one more physical meaning*: it is the average number of probing gas layers in the pore cross-section. In other words, the average *number of probing gas layers* is determined by the average pore *shape*.

As mentioned above, if the D_p value is not given in the work under study, then V_p/S_{BET} can be used instead and (use kinetic diameters σ of the nitrogen probing gas-0.364 nm and stored gases: hydrogen-0.289 nm, methane-0.380 nm, and carbon dioxide-0.330 nm) the average number of layers of these gases in pore cross-section, which (number) is simultaneously a dimensionless pore shape factor, can be estimate

$$F_d = \tau/\sigma \tag{4}$$

For $1 < F_d < 2$, one of the pore shape models can be represented by two layers of molecules with some *distance* between neighboring molecules in the bottom row (in contrast to the BET assumption); the molecules of the upper layer are partially immersed between molecules of the lower layer. If they are completely immersed, we get one layer (linear packing) and $F_d = 1$; if they do not sink at all, we have two parallel layers and $F_d = 2$ (square packing). When they are partially submerged, we have a triangle packing of molecules inside a smooth-walled split pore (note the packing of molecules, not the shape of the pore [12]). The case $F_d <$ 1 means either one layer of molecules with some distance between them, or gas molecules trapped between layers of a layered adsorbent.

Another imaginary model of pores can be a "stalactite cave", pores with rough walls, in which, at some small distance between the roughness peaks of opposite walls, overlapping forces arise to attract gas molecules. Such a model can fit any F_d. Another molecular packing model that seems to be acceptable for MOF and COF is the Chinese cherry with pinpoint adsorption active places.

2.3. Elimination of Fluctuations in the Density of the Sorbent in a Series of Samples

Excluding the gram in dimension of adsorbent capacity G, g/g, gives: 1) G/S_{BET},

g/m^2, surface activity, which indicates whether we need to activate the surface, for example by depositing some amount of metal to provide an H_2 spillover [15], 2) G/V_p, g/cm^3, a kind of volumetric capacity, 3) conditional G/V_{mi}, g/cm^3, imaginary filling of micropores, provided that the total amount of gas fills the pores of a certain volume (V_{mi}, V_{me}, etc.). Comparing these capacities, we can detect the location of micropore, in form of either cracks or pits on the surface of larger micropores or mesopores.

3. Discussion

3.1. Forces of Attraction and Repulsion of the Pore Wall

1) K. Xia *et al.* [16] activated by CO_2 mesoporous carbon SMK-3 at a temperature of 1223 K for 2, 4, 6, and 8 h to store hydrogen. Activation time was the only variable. With its increase, the adsorption of H_2 G, wt.% (1 bar/77 K), the total surface area S_{BET}, the total volume V_p, the volumes of micropores $V_{<2\ nm}$, $V_{1\text{-}2\ nm}$, $V_{<1\ nm}$ and their diameter DHK increase.

The *surface activity* G/S_{BET} decreases, so the increase in G is associated with all micropore volumes (directly proportional). The best correlation (R^2 = 0.9995) shows G vs. $V_{<1\ nm}$. G versus diameter D_{HK} gives a *direct* proportionality, which contradicts the idea of attraction. So, we tested *the generalized size* $\tau = V_p/S_{BET}$ (**Figure 1**).

It can be seen from **Figure 1** that a decrease in the generalized pore size from 1.1 to 0.95 nm leads to a strong increase in H_2 adsorption (according to the attraction effect [4]), but then (from 0.95 to 0.76 nm) adsorption slows down. It is obvious that repulsive forces arise, and V_p/S_{BET} = 0.95 nm is some critical value for this material and gas.

Imagine the density of a gas under the condition that the amount of gas G fits *completely* into the pores of a given size (**Table 1**). Pores > 2 nm were called

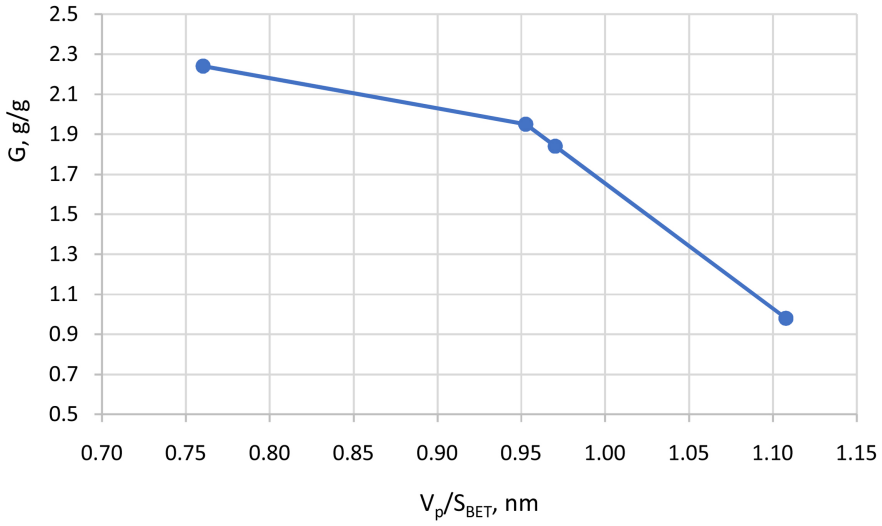

Figure 1. Effect of generalized carbon pore size V_p/S_{BET} on H_2 adsorption (1 Bar/77 K). Based on the data K. Xia *et al.* [16].

Table 1. Imaginary density G/V, g/cm³, of a gas that completely fills pores of a given size. Based on the data K. Xia *et al.* [16].

Sample	G,	$G/V_{<1\ nm}$,	$G/V_{1\div2\ nm}$,	$G/V_{<2\ nm}$,	G/V_{me},	G/V_p,
	wt.%	g/cm³	g/cm³	g/cm³	g/cm³	g/cm³
CMK-3	0.98	6.53	4.45	2.65	1.36	0.90
C-1223-2	1.84	6.57	4.49	2.67	1.72	1.05
C-1223-4	1.95	6.50	3.98	2.47	1.6	0.97
C-1223-6	2.24	6.59	3.61	2.33	1.98	1.07
Average	1.75	6.55	4.13	2.53	1.67	1.00
STD, %	30.92	0.60	10.10	6.26	15.52	7.83

G: capacity, V: volume of pores, subscript: pore size.

mesoporous, and their volume V_{me} was obtained as $V_{me} = V_p - V_{<2\ nm}$. Note that the serial STD of all discussed volumes $V_{<1\ nm}$, $V_{1\div2\ nm}$, etc. as well G, are in the range of 21% ÷ 38%.

First of all, let's compare STD of gravimetric G (30.92%) and volumetric G/V_p (7.83%) capacities. Excluding gram of carbon from the dimension of the uptake G allows to reduce STD by 4 times; this means that the time of carbon activation significantly affects the density of carbon. The average G/V data illustrate the decrease in gas density with increasing pore size. Impressive is STD (only 0.6%) $G/V_{<1\ nm}$, which can be explained by the attraction of gas by the walls; the highest STD shows G/V_{me} where there is no gas attraction.

2) Texier-Mandoki *et al.* [17] presented uptakes H_2 by 7 carbon species at 77 K and pressures 1, 3. 7 and 10 bars; given are S_{BET} and V_p obtained by low temperature adsorption of N_2; D_p is missing. We calculate the average layer thicknesses N_2 $\tau = V_p/S_{BET}$, nm, take them as estimates of pore sizes and then calculate the pore shapes (H_2 molecules packings) $F_d = \tau/\sigma_H$ (σ_H = 0.289 nm is the kinetic diameter of H_2 molecules). **Figure 2** shows dependencies H_2 uptakes G, wt.%, on the pore size (left) and on the H_2 molecules packing τ/σ_H (right).

It can be seen from **Figure 2** (left) that in the narrowest pores (0.46 nm) the walls have a *repulsive* effect on gas molecules and uptake is low; an increase in pressure suppresses repulsive forces and increases absorption. It can also be seen that, starting from a pore size of 0.53 nm, G, wt.%, is inversely proportional to the size.

Figure 2 (right) shows the effect of the number of gas layers (packing of gas molecules in layers) on G. Noteworthy are two packings of H_2 molecules: 1.63 and 1.85, which ensure high adsorption. Packing between them, F_{dh} = 1.7, is a special case, it gives markedly lower uptake (the sample is Norit R0.8 carbon). This result can be explained by the presence of *two* PSD peaks (see [18], Fig. 2) at pore diameters $d_1 < 0.49$ nm and $d_2 > 0.49$ nm, which gives an average value of $d = 0.49$ nm; both real diameters impair adsorption.

Returning to the work of Fiero [8], mentioned in the introductory part, we

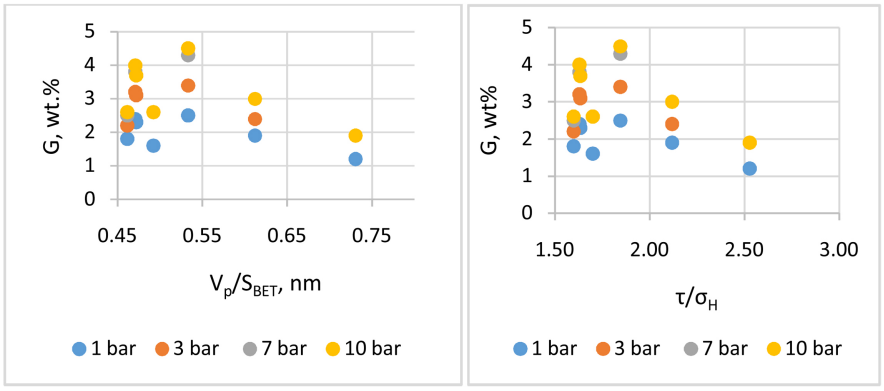

Figure 2. Adsorption of H_2 by 7 carbon species at 77 K and 4 pressures. Dependence of uptake G on the generalized pore size V_p/S_{BET} (left) and on the average number of H_2 layers τ/σ_H (right). Based on the data of Taxier-Mandoki *et al.* [17].

believe that the decrease in the absorption of H_2 at a very large (excessive) surface area and volume of micropores is explained by the formation of micropores of such small sizes that repulsive forces appear.

3) Sun *et al.* [19] noted that ultra-micropore sorbent (<0.7 nm) should be avoided for *natural gas* storage. Obviously, for methane the forces of attraction act in the range of pore diameters range of 0.7 [19] ÷ 1.3 [1] nm.

3.2. The Sorbent Energy P_mV

1) Examples of P_mV constancy for various volumes in conventional catalysts and sorbents are given in author's report [SI-1]. The report is given in SI form because the publisher did not refer to it, and the only evidence in English for its existence is the review by Shchukin *et al.* [20].

2) Valekar *et al.* [21] obtained by wet granulation the spheres from MOFs: MIL-100(Fe), MIL-101(Cr), UiO-66(Zr), and UiO-66(Zr)_NH_2 with ρ-Al_2O_3 as a binder. Total surface area S_{BET} (m^2/g), total pore volume V_p (cm^3/g) from low-temperature N_2 adsorption, and sphere crushing strength P_m(N) are given. We tested correlations of P_m with S_{BET}, V_p and V_p/S_{BET}; no correlations were found. In the same time the sorbent energy P_mV_p showed close relationships with S_{BET} (logarithmic function, $R^2 = 0.819$) and especially with size V_p/S_{BET} (**Figure 3**).

Figure 3 (left) reflects the effect of pore size reduction on increased attraction of gas molecules. **Figure 3** (right) shows that the energy of the material is inversely proportional to and closely related to the packing of N_2 molecules ($R^2 = 0.975$). It is noteworthy that the maximum energy (point 1.19/6.56) corresponds to $\tau/\sigma \approx 1$, *i.e.*, to the pore shape F_d which provides a single-layer packing of N_2 molecules.

3) Dhainaut *et al.* [22] tested tablets hardness P_m (N) of MOFs: UiO-66, UiO-66-NH2, UiO-67, and HKUST-1. As displacement V for P_mV, the given S_{BET}, V_{mi}, S_{BET}/V_{mi}, crystal density and bulk density of tablets can be tested. We also note two facts related to V_{mi}: 1) V_{mi} of powders and tablets, made from

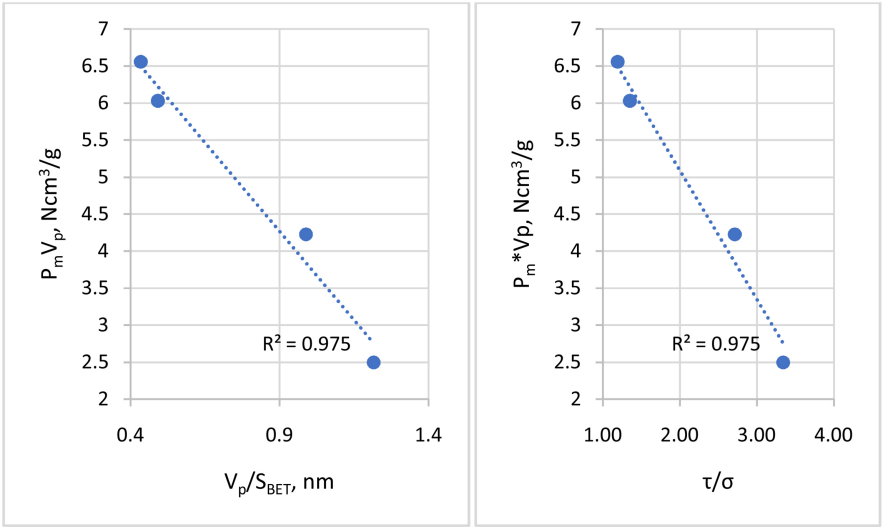

Figure 3. MOF. Correlations between sorbent energy $P_m V_p$ and a size V_p/S_{BET} (left); $P_m V_p$ and packing of N_2 molecules (number layers τ/σ, right). Based on the data from Valekar *et al.* [21].

them, are about equal (see also **Table 3**), 2) generalized micropore size (thicknesses of probing gas) V_{mi}/S_{BET} are almost equal for all powder and tablet samples. To find samples with close sorbent energy $P_m V$ graphs like **Figure 4** were plotted.

On **Figure 4** the highest $P_m S_{BET}$ has UiO-67. Similar plot with highest (but little lower) energy for the same sorbent was obtained for displacement V_{mi} (not shown). According to authors ([22], Fig. S6) this MOF possess the highest volumetric capacity.

3.3. Gas Energy

Mahmoud [23] in a review, on *methane* storage, gave total and deliverable uptakes, pressure and temperature for 15 MOFs samples, 12 porous organic polymers (POP) and 20 AC samples, their S_{BET} and V_p. D_p is missing, so we used V_p/S_{BET}. For MOF volumetric G, cm³/cm³, for POPs and AC, gravimetric G, g/g, capacities are presented.

a) MOF. G versus V_p, $V_p(P/T)$, S_{BET}, $S_{BET}(P/T)$ and V_p/S_{BET}.

Among the 15 experiments with MOF, the closest dependence shows deliverable G, cm³/cm³, on the total pore volume V_p (**Figure 5**, left).

On **Figure 5** left, the only separated point (0.94/306) belongs to the sample MOF-519 with the highest pressure in the series of 250 Bar. After excluding this sample, the remaining samples form a straight regression line with $R^2 = 0.8918$. The gas energy $V_p(P/T)$, as an independent variable (**Figure 4**, right), returns MOF-519 in the MOF family, but separates samples ST-2 (200 Bar/303 K, 200 Bar/289 K). After excluding ST-2, the rest of the samples form a straight line with $R^2 = 0.8849$. The absence of points between the MOF-519 and ST-2 samples on this graph suggests that $G = 306$ cm³/cm³ is the maximum possible capacity

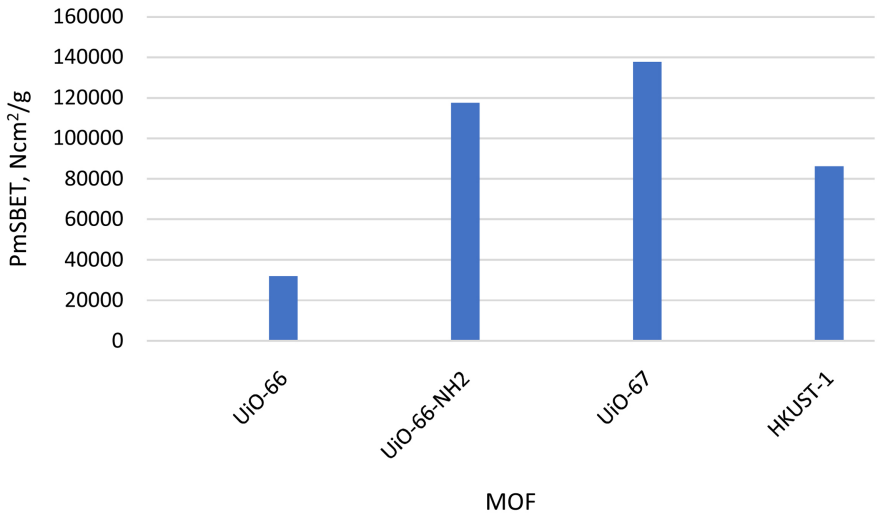

Figure 4. Tableted MOF sorbents energy $P_m{}^*S_{BET}$; P_m is hardness (N) and S_{BET} is total surface area m^2/g. Based on the data from Dhainaut *et al.* [22].

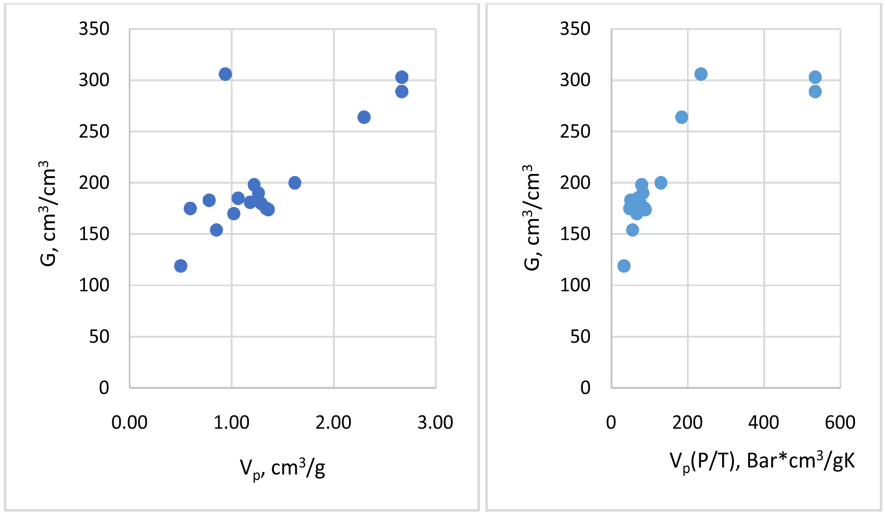

Figure 5. Dependence of the deliverable capacity G of the MOF on the pore volume V_P (left) and on the gas energy $V_p(P/T)$ (right). Based on the data from Mahmoud review [23].

for the studied MOFs; at very high pressure (dense gas), repulsive forces prevent the capacitance from growing.

When S_{BET} was taken as the displacement, the variable $S_{BET}(P/T)$ combined all the samples into one line G-s (not shown), but with a noticeably larger scattering, $R^2 = 0.7591$. With the exception of MOF-519, which is furthest from the line, $R^2 = 0.8324$ was obtained, which is less than for G vs. $V_p(P/T)$.

G, cm^3/cm^3, depending on another displacement, the size V_p/S_{BET}, is shown in Figure 6.

Figure 6 shows the absence of any relationship between the capacity of this series of MOF and the pore size. The separated point (0.15/175) is Cu-tbo-MOF 5 material (see below).

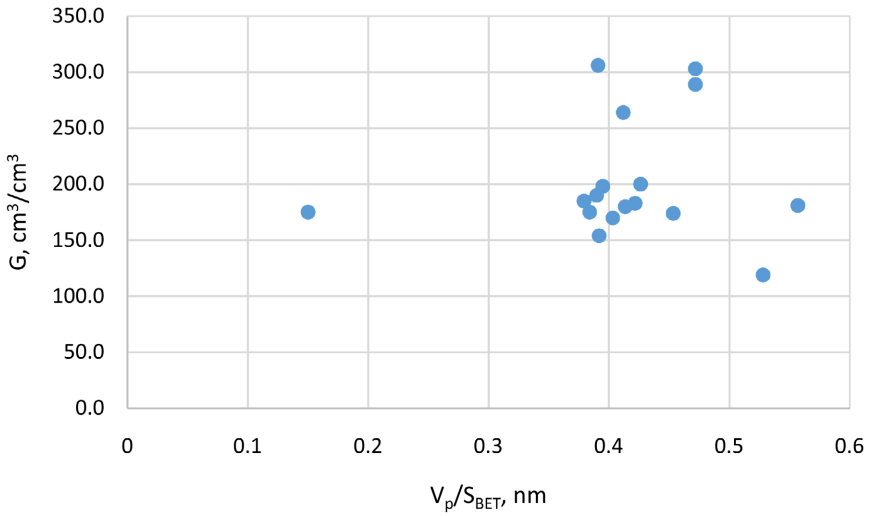

Figure 6. MOF. G vs. V_p/S_{BET}. Based on the data from Mahmoud review [23].

The packing of CH_4 molecules (number of layers) τ/σ.

In this MOF series, the τ/σ range is 0.39 ÷ 1.47. The smallest value $\tau/\sigma = 0.39$, the only value < 1, belongs to the mentioned Cu-tbo-MOF 5 sample. This MOF is characterized by "the presence of very strong CH_4 adsorption sites near the organic linker with similar adsorption energetics as the open metal sites" [24]. This packing of knots and molecules resembles a Chinese cherry or a stalactite cave with repeatedly changing distances between floor and ceiling; both can serve as pore models. From the remaining data τ/σ (1.00 - 1.47) it can be concluded that these samples have a flat split shape, allowing 1 ÷ 1.5 layers of methane molecules.

b) POP.

The dependences of G, g/g, on S_{BET} and V_p are directly proportional with R^2 = 0.9465 and 0.79 correspondingly. The gravimetric capacity G, g/g, makes it possible to estimate the *surface activity* G/S_{BET}, g/m^2; the most active surface has COF-5. Graphs of G vs. $S_{BET}(P/T)$ and vs. $V_p(P/T)$ look like in **Figure 5** (left); "pushed out" sample from the series, is PPN-4. Excluding this sample, we get straight lines with R^2 = 0.9787 and R^2 = 0.9033 for G vs. $S_{BET}(P/T)$ and G vs. $V_p(P/T)$ respectively, *i.e.* values higher than for G depending on S_{BET} and V_p.

There was no evidence of an effect of V_p/S_{BET} pore size on G, g/g. Assuming that this is due to fluctuations in the density of POPs, the gravimetric uptake of methane G, g/g, was related to cm^3 of the total pore volume V_p, cm^3/g. G/V_p, g/cm^3, kind of volumetric capacity. The plot of G/V_p versus V_p/S_{BET} was approximated by a power function (**Figure 7**).

Figure 7 shows a very sharp increase in volumetric capacity as a result of a decrease in pore size. Although the relationship between the variables does not seem very strong (R^2 = 0.7338), the exclusion of the not very important (due to high V_p/S_{BET}) COF-5 sample (point 0.77/0.144) raises R^2 to 0.8483.

c) Activated carbons.

The processing conditions were: constant P = 35 Bar and T = 296 ÷ 300 K (practically constant), so the gas force in Equation (1) was constant. The

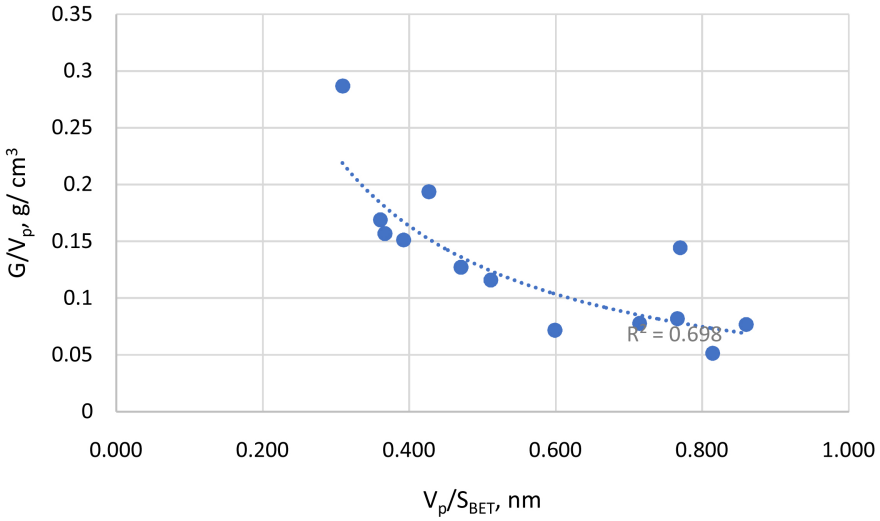

Figure 7. POPs. Effect of the generalized pore size V_p/S_{BET} on the volumetric capacity G/V_p. Based on the data from Mahmoud review [23].

strengths of the connections (R^2) between G and displacements S_{BET}, V_p and V_p/S_{BET} were tested (**Table 2**).

Among the AC samples, MAXSORB – 3 has the highest S_{BET} = 3140 m^2/g and lowest V_p= 0.179 cm^3/g, which gives the smallest generalized pore size V_p/S_{BET} = 0.057 nm (0.15 methane layers). The latter may explain the highest G = 0.408, g/g, of this sample and suggest a *stalactite pore model*. Use the volumetric delivery capacity G/V_p, *i.e.*, elimination of fluctuations in sorbent density, provides a very strong relationship (R^2 = 0.9658) between this capacity and pore size V_p/S_{BET}.

Fomkin *et al.* [25] studied the adsorption of H_2 G, wt.%, by 5 different carbon materials at 3 combinations (a, b, c) of pressure and temperature (P/T):$(P/T)_a$ = 1.01 Bar/20.38 K = 0.050, $(P/T)_b$ = 100 Bar/303 K = 0.330, and $(P/T)_c$ = 200 Bar/393 K = 0.509. So, P/T was processing generalized variable. The S_{BET} and V_{mi} of the samples were measured by the adsorption of N_2 and benzene, respectively.

The S_{BET} and V_{mi} of the samples fluctuated markedly: the STDs were 37% and 68%, respectively. Therefore, as an independent textural characteristic of the AC samples, we took the surface topography (roughness) [1] V_{mi}/S_{BET}, cm^3/m^2, the STD of which was lower (29%). The dependent variable was the energy in the form $G(P/T)$ and for each (P/T) the behavior of the function $G(P/T) = f(V_{mi}/S_{BET})$ was studied; shapes of curves were similar. For compactness, in order to fit all the data on one graph, the *average* $G(P/T)$ values for each P/T were calculated, individual $G(P/T)$ were divided by average (normalized, subscript n) and normalized $G(P/T)_{na}$, $G(P/T)_{nb}$ and $G(P/T)_{nc}$ were plotted as functions of V_{mi}/S_{BET} (**Figure 8**).

It can be seen that the shapes of curves are similar. The closest are curves for P/T: 0.0500 and 0.509. This is one more example of similarity in PM [1].

Bambalaza *et al.* [26] compared the absorption H_2 by MOF UiO-66 both by powder and by the same material pressed into granules. Two series of adsorption

Table 2. Strength of correlations between AC textural properties and CH_4 capacities. Based on the data from Mahmoud review [24].

Dependence	Separated sample	Function	R^2
G, g/g, versus S_{BET}, m^2/g	none	polynomial	0.7977
G, g/g, versus V_p, cm^3/g	MAXSORB-3	Linear (rest)	0.4338
G, g/g, versus V_p/S_{BET}, nm	none	power	0.6072
G/V_p, g/cm^3 versus V_p/S_{BET}, nm	none	power	0.9658

G, capacity, V_p, S_{BET}, total pore volume and surface area, R-squared values represent the scatter around the regression line.

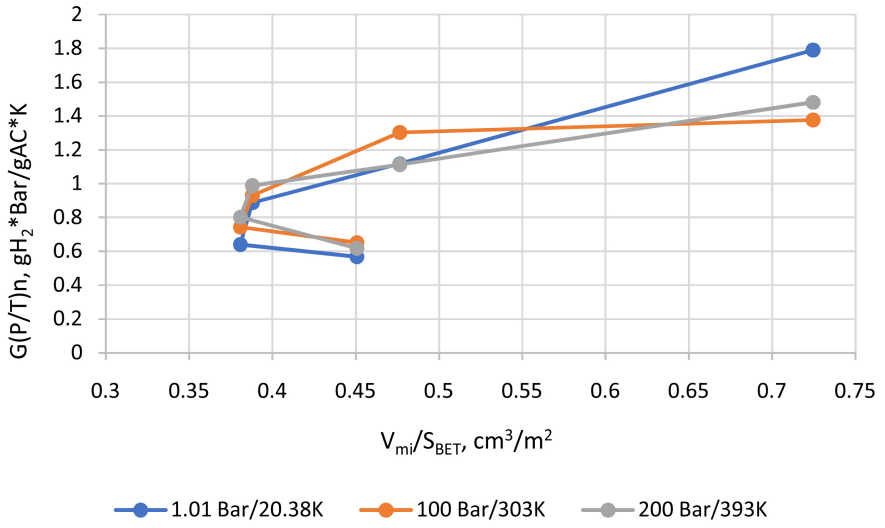

Figure 8. Dependences of the normalized energies $G(P/T)_n$ on the surface roughness V_{mi}/S_{BET} for 3 thermobaric conditions and 5 adsorbents. Based on the data Fomkin *et al.* [25].

carried out at temperatures: 77 K (dense gas) and 298 K (≈ STP gas); pressures varied from 0 to 100 Bar. On Fig. 3 (left) in [25] shows that a dense gas at high pressure experiences repulsive forces (absorption decreases), but we want also to know the effect of micropore sizes.

Textural parameters: S_{BET}, V_p, S_{mi}, V_{mi} and PSD are given, but the average values of D_p and D_{mi} are missing. Thus, we have used the generalized average pore size V_p/S_{BET} and the micropore size V_{mi}/S_{mi}, which are the thicknesses of the N_2 gas layers. Dividing the sizes by the kinetic diameters of N_2 and H_2 we obtain the average shape factors of pores and micropores (numbers of layers) F_{dn}, F_{dh}, *i.e.*, packings of N_2 and H_2 molecules (subscripts n and h correspondingly) (**Table 3**).

It follows from the table that tableting the powder did not lead to a change in the micropore size V_{mi}/S_{mi}. This closeness is confirmed by the PSD peaks (Fig. 2 in [25]); in the region of micropores, the pore sizes are very close for powder and tablets (3 pairs: d_1 = 0.6 and 0.6 nm, d_2 = 0.70 and 0.76 nm, and d_3 = 1.35 and 1.35 nm, respectively). Assuming a constant V_{mi}/S_{mi} and using the indicated sizes, we can estimate the individual micropore shape factors f_{d1n}, f_{d2n} and f_{d3n}

(Table 3).

The value of the total packings F_{dn}, F_{dh} in pellets are higher than in powder, while the packings in micropores f_{dn}, f_{dh} have not changed.

The correlations between gas energy $V_P(P/T)$ and gas uptake by powder and pellets were checked using the ratios the pellet parameters to powder parameters (Pellet/Powder) (Table 4).

The pellet gas energy is 0.84 of the powder energy at both temperatures. This value is close (0.82) to the reduction in both *total* and *excess* uptake at 298 K. The lack of correlation at 77 K for both total uptake and excess led us to the idea of introducing a *residual* amount of gas, which is the difference between the total uptake and excess. As can be seen, the decrease in the amounts of residual gas correlates with the energy of the gas at both temperatures.

Gomez-Gualdrón *et al.* [7] tested H_2 cryo-adsorption using the MOF series: NU-1101, NU-1102, and NU-1103, cycling between 100 Bar/77 K and one of two delivery conditions: 5 Bar/77 K and 5 Bar/160 K. Most of the data were obtained both experimentally and by simulations. We took for analysis, as a rule, the experimental data; from those obtained by simulation, we took the smallest d and largest D pore sizes as well as heat of adsorption Q_a. Effect of gas energy $V_P(P/T)$ on the total gravimetric capacity G is shown on Figure 9. Exactly the same dependences (not shown) were got for excesses at 5 Bar/77 K and at 5 Bar/160 K.

From the 9 graphs it follows that the largest both total and deliverable capacities correspond to the highest energy of the gas.

Table 3. Textural properties of MOF UiO-66 powder and pellets. Based on the data of Bambalaza *et al.* [26].

MOF state	V_P/S_{BET}	V_{mi}/S_{mi}	F_{dn} total	f_{dn} micro	F_{dh} total	f_{dh} micro	$f_{d1.n}$	$f_{d2.n}$	$f_{d3.n}$
	nm	nm	---	---	---	---	---	---	---
Powder	0.55	0.38	1.52	1.055	1.91	1.331	1.559	1.819	3.508
Pellets	0.47	0.38	1.30	1.057	1.64	1.329	1.562	1.979	3.515

V_P, S_{BET}, total pore volume and surface area, V_{mi}, S_{mi}, micropore volume and surface area, F_d, f_d, molecules packing: F, total, f, inmicropores pore, n, nitrogen, h, hydrogen.

Table 4. Gas energy $V_P(P/T)$ and gravimetric amount H_2 stored by powder and pellets under pressure P = 100 Bar, temperatures 77 K and 298 K at different stages of storage. Based on the data of Bambalaza *et al.* [26].

MOF state	$V_P(P/T)$, cm^3 Bar/gK		Gravimetric uptake, wt.%					
			Total at T		Excess at T		Residual at T	
	77 K	298 K	77 K	298 K	77 K	298 K	77 K	298 K
Powder	1.25	0.32	5.0	1.1	2.1	1.1	2.9	0.7
Pellets	1.05	0.27	5,1	0.9	2.7	0.9	2.4	0.6
Pellet/Powder	0.84	0.84	1.02	0.82	1.29	0.82	0.83	0.86

V_P, total pore volume, P, pressure, T, temperature.

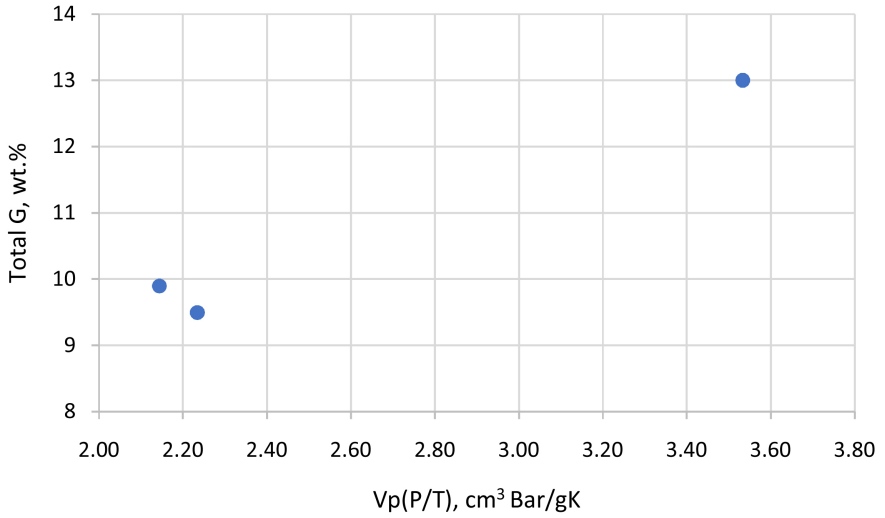

Figure 9. Effect of gas energy $V_p(P/T)$ on the total capacity of storage adsorbents (from left to right) Nu-1102, Nu-1101 and Nu-1103 at 100 bar/77 K. According to Gomez-Gualdron *et al.* [7].

Table 5. MOF pore shape factors and packings of H_2 molecules. Based on simulated (d, D) and experimental (S_{BET}, V_p) data from Gomez-Gualdrón *et al.* [7].

MOF	Smallest d pore diameter	Largest D pore diameter	V_p/S_{BET}	F_d of smallest pore	F_d of largest pore	Packings in		
						Small d	Large D	Average
	nm	nm	nm	---	---	---	---	---
Nu-1101	0.95	1.72	0.40	2.4	4.3	3.29	5.95	1.37
Nu-1102	1.11	2.05	0.44	2.5	4.6	3.84	7.09	1.53
Nu-1103	1.35	2.42	0.44	3.1	5.6	4.67	8.37	1.51

F_d, dimensionless pore shape factor, V_p, S_{BET}, total both pore volume and surface area, Packing is number H_2 molecules across pore size.

The reported total surface area S_{BET} and volume V_p, as well as the diameters of the smallest d and largest D pores, make it possible to estimate the dimensionless shape factors (the number of layers N_2) F_d of these pores and the packing of hydrogen molecules in them (kinetic diameter $\sigma = 0.289$ nm).

Comparing d and D with V_p/S_{BET} in the Table 5, it can be concluded that the proportions of both the smallest and largest pores are very small. F_d-s says that Nu-1101, Nu-1102 have split ($F_d \approx 2$) smallest and circular ($F_d \approx 4$) largest pores, while Nu-1103 has the smallest pores, having ≈ 50:50% split/circular motifs, and the largest pores with ≈ spherical shape. The average thicknesses of the N_2 layer (0.40 ÷ 0.44 nm) and the numbers of H_2 layers (packings) are almost the same (1.37 ÷ 1.53).

The dependences of the heat of adsorption Q_a on both diameters d and D (all received by simulation) have the form of straight lines with equidistant points and equal gradients, *inversely* proportional and having strong correlations: R^2 =

0.954 for d and $R^2 = 0.982$ for D. It is possible that small pores are located inside the largest ones. The dependence of Q_a on the experimental V_p/S_{BET} looks different, namely, as a graph in **Figure 9** rotated counterclockwise to 180˚, *i.e.*, confirms that the smaller the pore size, the higher the heat of adsorption.

4. Conclusions

The generalized variables proposed for gas storage adsorbents reveal a number of new facts. On the dependence of the storage capacity H_2 on the generalized pore size, the critical size is found; at this size, the action of attractive forces on gas molecules decreases and the action of repulsive forces begins. At very high pressure, the repulsive forces prevent the capacitance from growing.

Series of MOF show independence of volumetric capacity on generalized pore size but for POPs and ACs, this dependence exists. For *granular* MOFs, the sorbent energy (crush strength times volume) is inversely proportional to and closely related to pore size. The maximum energy corresponds to the shape of the pores, which provides a single-layer packing of molecules. For MOF *tablets*, the highest capacity corresponds to the highest product of hardness and surface area.

In *POP*s series, no relation between the *gravimetric* capacity and the pore size was found, but when gravimetric capacity is converted to volumetric one, a rather strong power-law dependence arises between them. The same thing happened with the carbon series.

It has been found that the energy of the gas can correlate with residual uptake better than with the total and delivery capacity.

Models of pores in the form of a Chinese cherry tree and a stalactite cave are proposed.

Article Highlights

Energy as a generalized product of force and displacement is applied to gas storage physical adsorbents: gas pressure forms gas energy; the mechanical strength of the molded adsorbent forms the energy of the sorbent.

Any textural property of the adsorbent: surface area, volume and size of pores (micropores) can be a displacement that provides the best correlation between energy and storage capacity.

The universal pore size for all porous materials is V_p/S_{BET}, the average layer of the probing gas.

An important result of converting a gravimetric capacity into volumetric capacity is the elimination of fluctuations in the density of the sorbent and, thereby, an improvement in the relationship between energy and capacity.

Declarations

No funds, grants, or other support was received.

Ethics Approval

No figures, tables or text passages have been used that require permission.

Conflicts of Interest

The author declares no conflicts of interest regarding the publication of this paper.

References

[1] Titelman, L. (2021) Generalized Parameters of Porous Materials as Similarity Numbers. *Advances in Materials Physics and Chemistry*, **11**, 177-201. https://doi.org/10.4236/ampc.2021.1111017

[2] Titelman, L. (2012) Generalized Processing-Structural Functions for Porous Materials. *Journal of Porous Materials*, **19**, 1-13. https://doi.org/10.1007/s10934-010-9440-y

[3] Titelman, L. and Levitskaya, N. (1987) Selective Effect of Technological and Operational Factors on the Mechanical Properties of Catalysts. *Russian Journal of Applied Chemistry* (*Zhurnal Prikladnoi Khimii*), **60**, 2666-2670. (In Russian)

[4] Dubinin, M.M. (1960) The Potential Theory of Adsorption of Gases and Vapors for Adsorbents with Energetically Non-Uniform Surface. *Chemical Reviews*, **60**, 235-266. https://doi.org/10.1021/cr60204a006

[5] Sethia, G. and Sayari, A. (2016) Activated Carbon with Optimum Pore Size Distribution for Hydrogen Storage. *Carbon*, **99**, 289-294. https://doi.org/10.1016/j.carbon.2015.12.032

[6] Duan, Z., Li, Y., Xiao, X., Huang, X., Li, X., Li, Y., Zhang, Ch., Zhang, H., Li, L., Lin, Z., Zhao, Y. and Huang, W. (2020) Interpenetrated Metal-Organic Frameworks with ftw Topology and Versatile Functions. *ACS Applied Materials & Interfaces*, **12**, 18715-18722. https://doi.org/10.1021/acsami.0c03336

[7] Gómez-Gualdrón, D., Wang, T., García-Holley, P., Sawelewa, R.M., Argueta, E., Snurr, R., Hupp, J., Yildirim, T. and Farha, O. (2017) Understanding Volumetric and Gravimetric Hydrogen Adsorption Trade-Off in Metal-Organic Frameworks. *ACS Applied Materials & Interfaces*, **9**, 33419-33428. https://doi.org/10.1021/acsami.7b01190

[8] Fierro, V., Zhao, W., Izquierdo, M.T., Aylon, E. and Celzard, A. (2010) Adsorption and Compression Contributions to Hydrogen Storage in Activated Anthracites. *International Journal of Hydrogen Energy*, **35**, 9038-9045. https://doi.org/10.1016/j.ijhydene.2010.06.004

[9] Goldsmith, J., Wong-Foy, A., Cafarella, M.J. and Siegel, D. (2013) Theoretical Limits of Hydrogen Storage in Metal-Organic Frameworks: Opportunities and Trade-Offs. *Chemistry of Materials*, **25**, 3373-3382. https://doi.org/10.1021/cm401978e

[10] Putz, A.-M., Cecilia, S., Ianăşi, C., Dudás, Z., Székely, K., Plocek, J., Sfârloagă, P., Săcărescu, L. and Almásy, L. (2015) Pore Ordering in Mesoporous Matrices Induced by Different Directing Agents. *Journal of Porous Materials*, **22**, 321-331. https://doi.org/10.1007/s10934-014-9899-z

[11] Gun'ko, V.M. and Mikhalovsky, S. (2004) Evaluation of Slitlike Porosity of Carbon Adsorbents. *Carbon*, **42**, 843-849. https://doi.org/10.1016/j.carbon.2004.01.059

[12] Azevedo, D.C.S., Rios, R.B., Lopez, R.H., Torres, A.E.B., Cavalcante, C.L., Toso, J.P. and Zgrablich, G. (2010) Characterization of PSD of Activated Carbons by Using Slit and Triangular Pore Geometries. *Applied Surface Science*, **256**, 5191-5197.

https://doi.org/10.1016/j.apsusc.2009.12.094

[13] Cárdenas, H. and Müller, E. (2021) How Does the Shape and Surface Energy of Pores Affect the Adsorption of Nanoconfined Fluids? *AIChE Journal*, **67**, e17011. https://doi.org/10.1002/aic.17011

[14] Bennett, Th., Cheetham, A., Fuchs, A. and Coudert, F.-X. (2017) Interplay between Defects, Disorder and Flexibility in Metal-Organic Frameworks. *Nature Chemistry*, **9**, 11-16. https://doi.org/10.1038/nchem.2691

[15] Han, Y.-J. and Park, S.-J. (2015) Effect of Nickel on Hydrogen Storage Behaviors of Carbon Aerogel Hybrid. *Carbon Letters*, **16**, 281-285. https://doi.org/10.5714/CL.2015.16.4.281

[16] Xia, K., Gao, Q., Wu, C., Song, S. and Ruan, M. (2007) Activation, Characterization and Hydrogen Storage Properties of the Mesoporous Carbon CMK-3. *Carbon*, **45**, 1989-1996. https://doi.org/10.1016/j.carbon.2007.06.002

[17] Texier-Mandoki, N., Dentzer, J., Piquero, T., Saadallah, S., David, P. and Vix-Guter, C. (2004) Hydrogen Storage in Activated Carbon Materials: Role of the Nano Porous Texture. *Carbon*, **42**, 2735-2777. https://doi.org/10.1016/j.carbon.2004.05.018

[18] McCallum, C., Bandosz, T., McGrother, S., Muller, E. and Gubbins, K. (1999) A Molecular Model for Adsorption of Water on Activated Carbon: Comparison of Simulation and Experiment. *Langmuir*, **15**, 533-544. https://doi.org/10.1021/la9805950

[19] Sun, J., Jarvi, T., Conopask, L., Satyapal, S., Rood, M. and Rostam-Abadi, M. (2001) Direct Measurements of Volumetric Gas Storage Capacity and Some New Insight into Adsorbed Natural Gas Storage. *Energy Fuels*, **15**, 1241-1246. https://doi.org/10.1021/ef010067n

[20] Shchukin, E., Margolis, L., Kantorovich, S. and Polukarova, Z. (1996) The Influence of the Medium on the Mechanical Properties of Catalysts. *Russian Chemical Reviews*, **65**, Article No. 813. https://doi.org/10.1070/RC1996v065n09ABEH000231

[21] Valekar, A., Cho, K.-H., Lee, U.-H., *et al.* (2017) Shaping of Porous Metal-Organic Framework Granules Using Mesoporous ρ-Alumina as a Binder. *RSC Advances*, **7**, 55767-55777. https://doi.org/10.1039/C7RA11764G

[22] Dhainaut, J., Avci-Camur, C., Troyano, J., Legrand, A., Canivet, J., *et al.* (2017) Systematic Study of the Impact of MOF Densification into Tablets on Textural and Mechanical Properties. *CrystEngComm*, **19**, 4211-4218. https://doi.org/10.1039/C7CE00338B

[23] Mahmoud, E. (2020) Evolution of the Design of CH_4 Adsorbents. *Surfaces*, **3**, 433-466. https://doi.org/10.3390/surfaces3030032

[24] Spanopoulos, I., Tsangarakis, C., Klontzas, E., Tylianakis, E., Froudakis, G., Adil, K., Belmabkhout, Y., Eddaoudi, M. and Trikalitis, P. (2016) Reticular Synthesis of HKUST-Like tbo-MOFs with Enhanced CH_4 Storage. *Journal of the American Chemical Society*, **138**, 1568-1574. https://doi.org/10.1021/jacs.5b11079

[25] Fomkin, A., Pribylov, A., Men'shchikov, I., Shkolin, A., Aksyutin, O., Ishkov, A., Romanov, K. and Khozina, E. (2021) Adsorption-Based Hydrogen Storage in Activated Carbons and Model Carbon Structures. *Reactions*, **2**, 209-226. https://doi.org/10.3390/reactions2030014

[26] Bambalaza, S., Langmi, H., Mokaya, R., Musyoka, N., Renad, J. and Khotseng, L. (2018) Compaction of a Zirconium Metal-Organic Framework (UiO-66) for High Density Hydrogen Storage Applications. *Journal of Materials Chemistry A*, **6**, 23569-23577. https://doi.org/10.1039/C8TA09227C

Nomenclature

AC: activated carbon
D_h: hydraulic circular pore diameter (m) = 4 V_p(m^3/g)/ S_{BET} (m^2/g)
D_p: pore size (nm)
F: generalized pore shape factor (nm*m^2/cm^3) = D_p (nm)* S_{BET} (m^2/g)/ V_p (cm^3/g)
F_d: generalized pore shape factor (dimensionless) = D_p (m)* S_{BET} (m^2/g)/ V_p (m^3/g)
G: capacity: gravimetric g/g, volumetric cm^3/cm^3
GP: generalized parameter
MOF: metal-organic framework
P: gas pressure
PM: porous material
P_m: mechanical strength of granule
POP: porous organic polymer
PSD: pore size distribution
S_{BET}: total specific surface area (m^2/g)
S_{mi}: micropore surface area (m^2/g)
StA: gas storage adsorbent
T: temperature
V: displacement (in Equation (1)), any pore surface area, volume, size.
V_{mi}: micropore volume (cm^3/g)
V_p: pore total specific volume (cm^3/g)
x: independent process variable
$\tau = V_p/S_{BET}$: the average thickness of the probing gas layers, nm

Supporting Information

SI, examples of $P_m V$ = const for various materials, mechanical test methods and pore volumes, from the author's report.